STRUCTURAL BIOLOGY COMMUNICATIONS

ISSN 2053-230X

Crystallographic snapshots of the EF-hand protein MCFD2 complexed with the intracellular lectin ERGIC-53 involved in glycoprotein transport

Tadashi Satoh,[a] Miho Nishio,[a] Kousuke Suzuki,[a] Maho Yagi-Utsumi,[a,b,c] Yukiko Kamiya,[a] Tsunehiro Mizushima[a] and Koichi Kato[a,b,c]*

[a]Graduate School of Pharmaceutical Sciences, Nagoya City University, 3-1 Tanabe-dori, Mizuho-ku, Nagoya, Aichi 467-8603, Japan, [b]Exploratory Research Center on Life and Living Systems (ExCELLS), National Institutes of Natural Sciences, 5-1 Higashiyama, Myodaiji, Okazaki, Aichi 444-8787, Japan, and [c]Institute for Molecular Science, National Institutes of Natural Sciences, 5-1 Higashiyama, Myodaiji, Okazaki, Aichi 444-8787, Japan. *Correspondence e-mail: kkatonmr@ims.ac.jp

Received 28 February 2020
Accepted 19 April 2020

Edited by A. Nakagawa, Osaka University, Japan

Keywords: cargo receptor; conformational polymorphism; crystal packing; glycoprotein transport; intracellular lectin; MCFD2; ERGIC-53.

PDB references: ERGIC-53–MCFD2, form 1, 4ygb; form 2, 4ygc; form 3, 4ygd; form 4, 4yge

Supporting information: this article has supporting information at journals.iucr.org/f

The transmembrane intracellular lectin ER–Golgi intermediate compartment protein 53 (ERGIC-53) and the soluble EF-hand multiple coagulation factor deficiency protein 2 (MCFD2) form a complex that functions as a cargo receptor, trafficking various glycoproteins between the endoplasmic reticulum (ER) and the Golgi apparatus. It has been demonstrated that the carbohydrate-recognition domain (CRD) of ERGIC-53 (ERGIC-53^{CRD}) interacts with N-linked glycans on cargo glycoproteins, whereas MCFD2 recognizes polypeptide segments of cargo glycoproteins. Crystal structures of ERGIC-53^{CRD} complexed with MCFD2 and mannosyl oligosaccharides have revealed protein–protein and protein–sugar binding modes. In contrast, the polypeptide-recognition mechanism of MCFD2 remains largely unknown. Here, a 1.60 Å resolution crystal structure of the ERGIC-53^{CRD}–MCFD2 complex is reported, along with three other crystal forms. Comparison of these structures with those previously reported reveal that MCFD2, but not ERGIC-53–CRD, exhibits significant conformational plasticity that may be relevant to its accommodation of various polypeptide ligands.

1. Introduction

Intracellular protein trafficking between organelles is ubiquitous in eukaryotic cells. Proteins are transported from the endoplasmic reticulum (ER) to the Golgi complex, undergoing various sugar modifications catalyzed by a variety of glycosidases and glycosyltransferases, and are then delivered to destinations inside and outside the cell (Kornfeld & Kornfeld, 1985). The delivery of cargo glycoproteins to transport vesicles is mediated by transmembrane cargo receptors with sugar-binding activity (Fiedler *et al.*, 1994; Hauri *et al.*, 2000).

In the early secretory pathway, the ER–Golgi intermediate compartment 53 protein (ERGIC-53) and vesicular integral membrane protein of 36 kDa (VIP36) function as cargo receptors between the ER and the Golgi apparatus (Fiedler *et al.*, 1994; Hauri *et al.*, 2000). ERGIC-53 and VIP36 share a homologous β-sandwich carbohydrate-recognition domain (CRD) with a structural resemblance (Velloso *et al.*, 2002; Satoh *et al.*, 2007) to legume lectins such as concanavalin A (Naismith & Field, 1996). Our previous sugar-binding profiling data demonstrated that ERGIC-53 and VIP36 interact with high-mannose-type N-linked oligosaccharides containing α-1,2-linked mannobiose or mannotriose structures (Kamiya *et al.*, 2005, 2008). ERGIC-53 is known to be involved in the intracellular transport of certain glycoproteins, such as

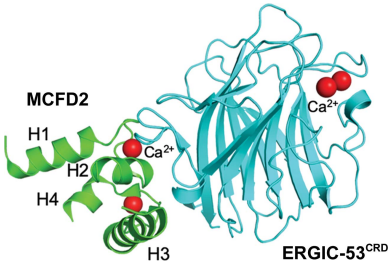

Table 1
Macromolecule-production information.

	Forms 1 and 4	Forms 2 and 3
Expression construct		
ERGIC-53^{CRD}	Residues 31–269	Residues 31–269
MCFD2	Residues 27–146 (full-length)	Residues 67–146 (N-terminally truncated)
Complete amino-acid sequence†		
ERGIC-53^{CRD}	MNHKVHMDGVGGDPAVALPHRRFEYKYSFKGPHLVQSDGTVPFWAHAGNAIPSSDQIRVAPSLKSQRGSVWTKTKAAFENWEVEVTFRVTGRGRIGA DGLAIWYAENQGLEGPVFGSADLWNGVGIFFDSFDNDGKKNNPAIVIIGNNGQIHYDHQNDGASQALASCQRDFRNKPYPVRAKITYYQNTLTVMIN NGFTPDKNDYEFCAKVENMIIPAQGHFGISAATGGLADDHDVLSFLTFQLTE	
MCFD2	MGHHHHHHHHHHSSGHIEGRHMLEEPAASFSQPGSMGLDKNTVHDQEHI MEHLEGVINKPEAEMSPQELQLHYFKMHDYDGNNLLDGLELSTAITH VHKEEGSEQAPLMSEDELINIIDGVLRDDDKNNDGYIDYAEFAKSLQ	MGHHHHHHHHHHSSGHIEGRHMLEMSPQELQLHYFKMHDYDGNNLLDG LELSTAITHVHKEEGSEQAPLMSEDELINIIDGVLRDDDKNNDGYI DYAEFAKSLQ

† The expression-tag sequence is underlined.

Table 2
Crystallization.

	Form 1	Form 2	Form 3	Form 4
Protein concentration (mg ml^{-1})	9.0	11.0	11.0	14.0
Buffer composition of protein solution	10 m*M* Tris–HCl pH 8.0, 10 m*M* $CaCl_2$	10 m*M* Tris–HCl pH 8.0, 10 m*M* $CaCl_2$, 2 m*M* FV peptide (929–937, SDLLLLKQS)	10 m*M* Tris–HCl pH 8.0, 10 m*M* $CaCl_2$, 2 m*M* FV peptide (929–937, SDLLLLKQS)	10 m*M* Tris–HCl pH 8.0, 10 m*M* $CaCl_2$,, 2.5 m*M* FVIII peptide (776–816)
Composition of reservoir solution	1.2 *M* sodium malonate, 0.5%(*v*/*v*) Jeffamine ED-2001, 50 m*M* Tris–HCl pH 7.0	17% PEG 8000, 8% ethylene glycol, 0.1 *M* Tris–HCl pH 8.5	19% PEG 3350, 8% ethylene glycol, 0.1 *M* bis-Tris pH 6.0	1.1 *M* sodium malonate, 0.5%(*v*/*v*) Jeffamine ED-2001, 0.1 *M* HEPES pH 7.0

cathepsin C, cathepsin Z, cathepsin-Z-related protein (Appenzeller *et al.*, 1999), blood coagulation factors V (FV) and VIII (FVIII) (Zhang *et al.*, 2003), Mac-2-binding protein (Mac-2BP)/galectin-3-binding protein (LGALS3BP) (Chen *et al.*, 2013; Fukamachi *et al.*, 2018) and α1-antitrypsin (AAT; Zhu *et al.*, 2018). ERGIC-53, but not VIP36, forms a stable complex with a 16 kDa soluble EF-hand Ca^{2+}-binding protein called MCFD2 (multi-coagulation factor deficiency 2; Zhang *et al.*, 2003). Accumulated evidence indicates that MCFD2 substantially contributes to the efficient secretion of several cargo proteins, including FV, FVIII (Zhang *et al.*, 2003), Mac-2BP/LGALS3BP (Chen *et al.*, 2013; Fukamachi *et al.*, 2018) and AAT (Zhu *et al.*, 2018). Indeed, combined deficiency of FV and FVIII (F5F8D), an autosomal recessive disorder characterized by coordinated reduction in the plasma levels of FV and FVIII, is caused by gene mutations in *MCFD2* as well as in *LMAN1* encoding ERGIC-53 (Zhang *et al.*, 2006, 2008).

To obtain structural insights into the transport functions of the ERGIC-53^{CRD}–MCFD2 complex, crystal structures of ERGIC-53^{CRD} bound to MCFD2 in the presence and absence of mannosyl oligosaccharide ligands have been determined (Satoh *et al.*, 2014; Nishio *et al.*, 2010; Wigren *et al.*, 2010). These structures, when compared with an uncomplexed MCFD2 structure in solution (Guy *et al.*, 2008), suggest that MCFD2, but not ERGIC-53^{CRD}, undergoes a conformational transition upon formation of the ERGIC-53^{CRD}–MCFD2 complex. The complexed structure provides a working model of cooperative interplay between ERGIC-53 and MCFD2. ERGIC-53 binds to N-linked glycans, whereas the allosterically activated MCFD2 binds polypeptide segments of cargo glycoproteins (Nishio *et al.*, 2010; Kamiya *et al.*, 2012). Crystal structures of sugar-bound ERGIC-53^{CRD}–MCFD2 complexes provide a structural basis for the recognition of N-linked glycoproteins by ERGIC-53 (Satoh *et al.*, 2014; Zheng *et al.*, 2013). A recent NMR study showed that MCFD2 interacts with peptide segment 807–816 of the B domain of FVIII through its canonical ligand-binding site (Yagi *et al.*, 2020). Although MCFD2 recognizes a similar sequence in the B domain of FV and presumably in other cargo glycoproteins, how MCFD2 recognizes various polypeptide ligands remains largely unsolved. Conformational variations of MCFD2, but not ERGIC-53^{CRD}, have been identified in ERGIC-53^{CRD}–MCFD2 complexes (Satoh *et al.*, 2014; Nishio *et al.*, 2010; Wigren *et al.*, 2010), suggesting conformational plasticity of MCFD2. However, these structures should be interpreted with great care because they could have been affected by the extent of crystal packing observed in their crystal structures.

We determined an improved 1.60 Å resolution crystal structure of the ERGIC-53^{CRD}–MCFD2 complex, in addition to three other crystal forms that contain MCFD2 structures with smaller crystal packing compared with previous crystal structures (Satoh *et al.*, 2014; Nishio *et al.*, 2010; Wigren *et al.*, 2010). Although the global structures of the complexes were similar to previously characterized structures, in our study we observed significant conformational polymorphism in MCFD2, but not in ERGIC-53^{CRD}, in their complexed states.

2. Materials and methods

2.1. Macromolecule production

Protein expression and purification of complexes between ERGIC-53^{CRD} (residues 31–269) and MCFD2 (full-length, residues 27–146; N-terminally truncated, residues 67–146)

Table 3
Data collection and processing.

Values in parentheses are for the outer shell.

	Form 1	Form 2	Form 3	Form 4
Diffraction source	BL5A, Photon Factory	BL44XU, SPring-8	BL44XU, SPring-8	BL44XU, SPring-8
Wavelength (Å)	1.0000	0.9000	0.9000	0.9000
Temperature (K)	95	95	95	95
Detector	ADSC Quantum 315r CCD	Rayonix MX225HE CCD	Rayonix MX225HE CCD	Rayonix MX225HE CCD
Space group	$P2_1$	$P2_1$	$P2_1$	$P3_121$
a, b, c (Å)	57.92, 116.93, 58.07	73.62, 168.89, 73.96	103.06, 58.77, 119.39	113.13, 113.13, 157.60
α, β, γ (°)	90, 120.13, 90	90, 119.86, 90	90, 109.01, 90	90, 90, 120
Resolution range (Å)	50–1.60 (1.63–1.60)	50–2.40 (2.44–2.40)	50–2.50 (2.54–2.50)	50–3.05 (3.10–3.05)
Total No. of reflections	318800	223803	167632	162674
No. of unique reflections	88266	61522	46552	22770
Completeness (%)	98.9 (100)	99.7 (100)	99.4 (97.8)	100 (100)
Multiplicity	3.7 (3.6)	3.7 (3.7)	3.6 (3.3)	7.1 (7.2)
$\langle I/\sigma(I)\rangle$	39.2 (3.4)	38.6 (9.8)	34.9 (8.8)	27.3 (7.6)
$R_{\rm r.i.m.}$†	0.069 (0.548)	0.066 (0.220)	0.059 (0.213)	0.126 (0.364)
Overall B factor from Wilson plot (Å^2)	19.58	32.98	28.84	25.54

† Estimated $R_{\rm r.i.m.} = R_{\rm merge}[N/(N-1)]^{1/2}$, where N is the data multiplicity.

Table 4
Structure refinement.

Values in parentheses are for the outer shell.

	Form 1	Form 2	Form 3	Form 4
Resolution range (Å)	20.00–1.60 (1.64–1.60)	20.00–2.40 (2.46–2.40)	20.00–2.51 (2.57–2.51)	20.00–3.05 (3.13–3.05)
Completeness (%)	98.8	99.6	98.6	99.9
σ Cutoff	None	None	None	None
No. of reflections				
Working set	82482 (6092)	57782 (4293)	43802 (2948)	21558 (1536)
Test set	4370 (328)	3081 (203)	2318 (157)	1162 (80)
Final $R_{\rm cryst}$	0.180 (0.233)	0.205 (0.261)	0.193 (0.242)	0.173 (0.236)
Final $R_{\rm free}$	0.199 (0.264)	0.246 (0.317)	0.232 (0.302)	0.173 (0.236)
No. of non-H atoms				
Protein	4062	9087	9252	6889
Ca^{2+}				
ERGIC-53$^{\rm CRD}$	0 [chains *A*/*C*]	8 [chains *A*/*C*/*E*/*G*]	8 [chains *A*/*C*/*E*/*G*]	3 [chains *A*/*C*/*E*]
MCFD2	4 [chains *B*/*D*]	8 [chains *B*/*D*/*F*/*H*]	8 [chains *B*/*D*/*F*/*H*]	6 [chains *B*/*D*/*F*]
Ligand	12	0	0	0
Water	239	238	293	10
Total	4317	9345	9564	6911
R.m.s. deviations				
Bonds (Å)	0.011	0.013	0.013	0.013
Angles (°)	1.437	1.509	1.533	1.642
Average B factors (Å^2)				
Protein	30.2	45.3	38.0	38.3
Ca^{2+}	23.6	43.0	35.2	40.5
Ligand	27.7	0.0	0.0	0.0
Water	39.6	40.1	32.8	17.2
Ramachandran plot				
Favored regions (%)	97.7	98.1	97.1	95.8
Additionally allowed (%)	2.1	1.8	2.8	4.1

were performed as described previously (Nishio *et al.*, 2010; Satoh *et al.*, 2014; Table 1). The purified ERGIC-53$^{\rm CRD}$–MCFD2 complexes were dissolved in 10 m*M* Tris–HCl pH 8.0 containing 10 m*M* $CaCl_2$.

2.2. Crystallization

Crystals were obtained under several crystallization conditions in the presence and absence of FV-derived and FVIII-derived peptides (Table 2). Initial crystallization screening was conducted by sitting-drop vapor diffusion using 1.0 µl volumes of protein solution and precipitant solution equilibrated against 100 µl of the latter. The crystallization conditions were optimized by hanging-drop vapor diffusion in the same manner as the sitting-drop experiments using a mother-liquor volume of 500 µl.

2.3. Data collection and processing

Crystals were cryoprotected with the crystallization solution containing 20% glycerol. Diffraction data were collected on the BL5A beamline equipped with an ADSC Quantum 315r

detector at the Photon Factory, Japan and on the Osaka University BL44XU beamline equipped with a Rayonix MX225HE CCD detector at SPring-8, Japan. Intensity integration and data scaling were performed using the *HKL*-2000 suite (Otwinowski & Minor, 1997). Data-collection statistics are given in Table 3.

2.4. Structure solution and refinement

Initial phase determinations were performed by the molecular-replacement method using *MOLREP* (Vagin & Teplyakov, 2010) and *Phaser* (McCoy *et al.*, 2007) with the reported trigonal structure (PDB entry 3a4u; Nishio *et al.*, 2010) as the search model. Further model building was performed manually using *Coot* (Emsley *et al.*, 2010). Subsequent refinements were performed using *REFMAC*5 (Murshudov *et al.*, 2011). The stereochemical quality of the final models was assessed using *MolProbity* (Chen *et al.*, 2010). The refinement statistics are summarized in Table 4. Structural superposition was performed with *SUPERPOSE* (Krissinel & Henrick, 2004). Molecular graphics were prepared using *PyMOL* (Schrödinger). Crystal contact areas were analyzed using *PISA* (Krissinel & Henrick, 2007).

3. Results and discussion

3.1. Structures of the ERGIC-53^{CRD}–MCFD2 binary complex

In this study, we determined four crystal structures of the ERGIC-53^{CRD}–MCFD2 complex, including an improved 1.60 Å resolution structure (Fig. 1), and found significant structural variations in MCFD2. Crystals of the ERGIC-53^{CRD}–MCFD2 complex were obtained under various crystallization conditions (termed 'crystal forms 1–4'). The ERGIC-53^{CRD}–MCFD2 crystals in crystal forms 1 and 4 contained two and three binary-complex molecules (termed 'complexes 1A–1B' and 'complexes 4A–4C') per asymmetric unit, respectively, whereas those in crystal forms 2 and 3 contained four binary-complex molecules (termed 'complexes 2A–2D' and 'complexes 3A–3D'). The ERGIC-53^{CRD}–MCFD2 complex contains four Ca^{2+} ions. Two Ca^{2+} ions bound to the sugar-binding site of ERGIC-53^{CRD} and two Ca^{2+} ions bound to MCFD2 (Satoh *et al.*, 2014; Nishio *et al.*, 2010; Wigren *et al.*, 2010). In the crystal form 1 structure (complexes 1A and 1B), the Ca^{2+}-binding sites of ERGIC-53^{CRD} were disordered despite having sufficient space for Ca^{2+} ions *in crystallo*. In crystal form 4 the Ca^{2+}-binding sites in ERGIC-53^{CRD} were partially disordered: complexes 4A and 4B contained two and one Ca^{2+} ions, respectively, whereas complex 4C had no bound Ca^{2+} ions. In contrast, in the crystal form 2 and 3 structures (complexes 2A–2D and 3A–3D) all four Ca^{2+} ions were observed in the ERGIC-53^{CRD}–MCFD2 complexes (Table 4). These data suggest that ERGIC-53^{CRD} tends to lose Ca^{2+} ions upon crystallization in comparison with MCFD2, consistent with the previous crystallographic study (Satoh *et al.*, 2014).

3.2. Crystal packing of MCFD2 complexed with ERGIC-53^{CRD}

To validate the structural variability of the ERGIC-53^{CRD}–MCFD2 complexes, the crystal contacts observed in molecules in the asymmetric and symmetry-related units were analyzed together with previously reported structures (Satoh *et al.*, 2014; Nishio *et al.*, 2010; Wigren *et al.*, 2010). The crystal contact areas are summarized in Supplementary Table S1.

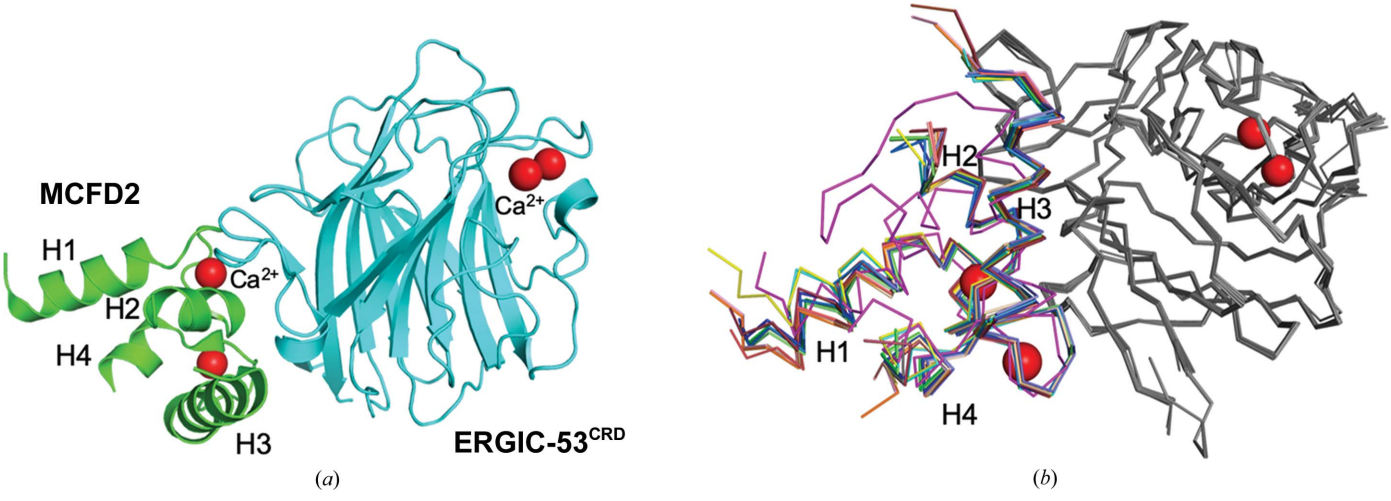

Figure 1
Structures of MCFD2 complexed with ERGIC-53^{CRD}. (*a*) A ribbon model of the ERGIC-53^{CRD}–MCFD2 complex is shown. ERGIC-53^{CRD} and MCMD2 are colored cyan and green, respectively. Bound Ca^{2+} ions are shown as red spheres. The positions of the helices (H1–H4) of MCFD2 are indicated. (*b*) Backbone-atom superimposition of ERGIC-53^{CRD}–MCFD2 crystal structures together with the apo MCFD2 NMR structure (PDD entry 2vrg, lowest-penalty model 1; Guy *et al.*, 2008). ERGIC-53^{CRD} structures are colored gray. MCFD2 structures are colored as follows: complex 1A, wheat; complex 1B, olive; complex 2A, blue; complex 2B, marine blue; complex 2C, slate; complex 2D, sky blue; complex 3A, raspberry; complex 3B, salmon; complex 3C, deep salmon; complex 3D, chocolate; complex 4A, green; complex 4B, lime; complex 4C, forest; PDB entry 3a4u (Nishio *et al.*, 2010), yellow; PDB entry 3lcp (Wigren *et al.*, 2010), chain *C*, orange; PDB entry 3lcp, chain *D*, pink; PDB entry 3wht (Satoh *et al.*, 2014), cyan. The solution structure of apo MCFD2 is colored magenta.

Notable differences existed in contact areas among all MCFD2 structures (445–992 Å^2). In complex 4A the total contact area was 444.8 Å^2 for MCFD2, suggesting that the MCFD2 structure in this crystal form is least affected by crystal packing *in crystallo*.

3.3. Comparison of MCFD2 structures derived from different crystal forms

The crystal structures of ERGIC-53^{CRD} in crystal forms 1–4 were quite similar to one another, with root-mean-square deviation (r.m.s.d.) values of 0.02–0.30 Å for the C$^{\alpha}$ atoms of the commonly observed residues (comprising amino-acid residues 44–129, 144–154, 162–170 and 186–268; Fig. 1*b*). In the improved 1.60 Å resolution structure, an alternative conformation of the Arg111 side chain of ERGIC-53^{CRD} was newly observed (Supplementary Fig. S1). In contrast, the crystallographic data from crystal forms 1–4 showed significant conformational variations of MCFD2, with r.m.s.d. values of 0.02–0.60 Å for the C$^{\alpha}$ atoms of the commonly observed residues (comprising amino-acid residues 76–97 and 112–142). In particular, the MCFD2 residues constituting the H1 and H4 helices and containing the Ca^{2+}-binding sites involved in interactions with ERGIC-53^{CRD} exhibited marked structural variations (Fig. 1*b*). Intriguingly, the potentially mobile segments are located in the ligand-binding site of MCFD2 (Yagi *et al.*, 2020), which corresponds to that of EF-hand proteins, as exemplified by calmodulin (CaM; Elshorst *et al.*, 1999; Fig. 2*a*). In the ligand-bound CaM complex, the H1, H2 and H4 helices are mainly involved in peptide-ligand binding (Elshorst *et al.*, 1999). These observations prompted an examination of the correlative helix angles (H1–H2 and H2–H4 helices) of MCFD2 derived from the 13 currently determined binary-complex structures together with previously reported structures, including apo MCFD2 solution structures (Satoh *et al.*, 2014; Nishio *et al.*, 2010; Wigren *et al.*, 2010). The comparative data indicated that the H1–H2 and H2–H4 helix angles are highly distributed around 32–42° (H1–H2) and 105–125° (H2–H4) (Fig. 2*b*). The correlative helix angles differed significantly between ERGIC-53^{CRD}-bound and unbound MCFD2 (Fig. 2*b*), as elucidated previously (Nishio *et al.*, 2010). The deviation of the helix angles of ERGIC-53^{CRD}-bound MCFD2 is higher than that of the unbound form, suggesting conformational plasticity of MCFD2 in the binary

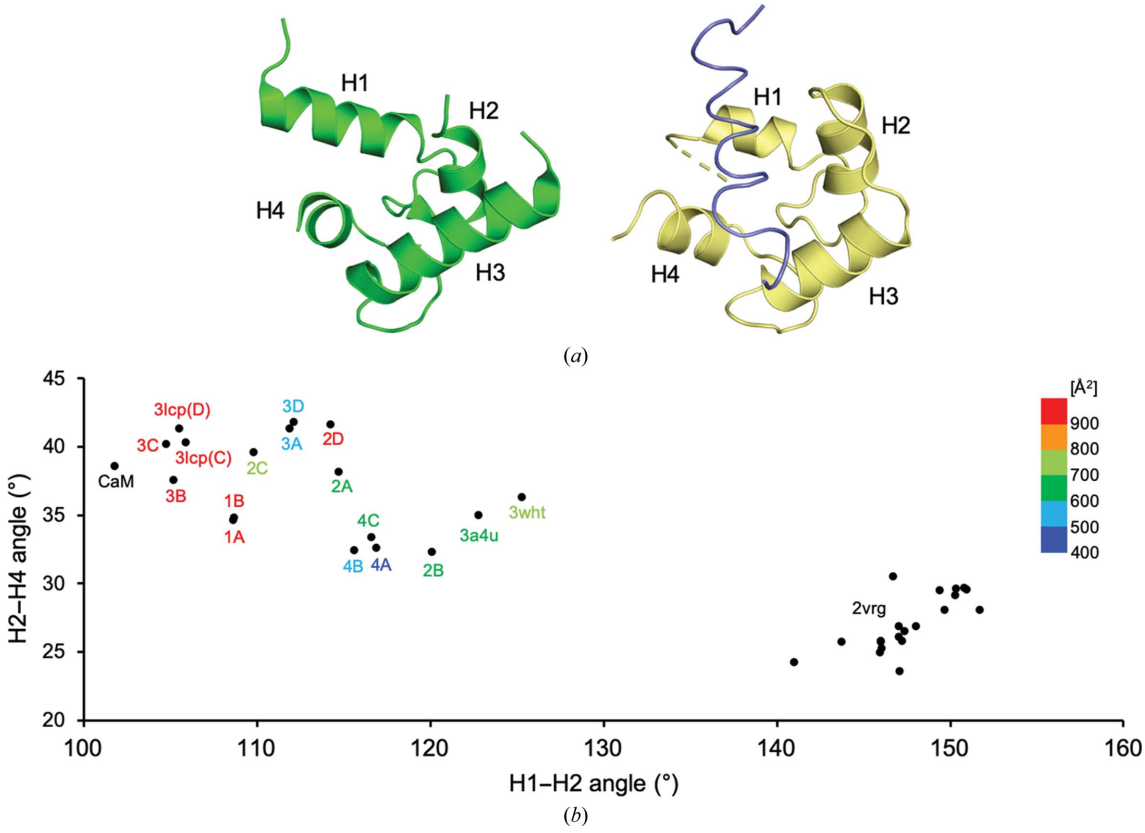

Figure 2
Conformational variations of the ligand-binding site of MCFD2. (*a*) Relative positions of helices H1–H4 in the EF-hand proteins MCFD2 and calmodulin. Structures of MCFD2 in complex with ERGIC-53^{CRD} (PDB entry 3a4u; Nishio *et al.*, 2010) and the ligand-bound calmodulin complex (PDB entry 1cff; Elshorst *et al.*, 1999) are shown on the left and right, respectively. The calmodulin and Ca^{2+}-pump peptide ligand structures are colored yellow and slate, respectively. (*b*) Correlative helix-angle distributions in the ligand-binding site of MCFD2. Vertical and horizontal axes indicate H2–H4 and H1–H2 helix angles, respectively. The data represent helix-angle conformations derived from currently determined MCFD2 structures together with previously reported MCFD2 and calmodulin structures, which are labeled with 'complex name', 'PDB code' or 'CaM', respectively, with a color gradient according to their crystal contact areas. For the apo MCMD2 NMR structure (PDB entry 2vrg; Guy *et al.*, 2008), the angles derived from the 20 lowest target-function structures are shown.

complex. The distribution pattern was not well correlated with the crystallization conditions, as exemplified by complexes 2A–2D and 3A–3D. However, there seems to be a relationship between the correlative helix angle and the crystal contact area, especially in the structures that possess larger contact areas (colored in red in Fig. 2*b*). Notably, the correlative helix angle derived from a ligand-bound CaM complex (Elshorst *et al.*, 1999) is similar to those from MCFD2 complexes with greater crystal-packing areas. Therefore, it is possible that the neighboring molecule in the crystal contacts the peptide-binding site of MCFD2, facilitating its conformational change towards the ligand-bound state *in crystallo*. Taken together with previous crystallographic observations (Satoh *et al.*, 2014; Nishio *et al.*, 2010; Wigren *et al.*, 2010), together with solution NMR data (Guy *et al.*, 2008), our findings indicate that the ligand-binding site of MCFD2 is allosterically activated by ERGIC-53^{CRD} upon complex formation, as suggested in our previous study (Nishio *et al.*, 2010). In this study, we revealed conformational variability of MCFD2, especially at its ligand-binding site, when in complex with its binding partner ERGIC-53. The conformational polymorphism of MCFD2 in the cargo-receptor complex may be relevant to its conformational adjustability in the recognition of various glycoprotein ligands.

Acknowledgements

We thank Kiyomi Senda and Kumiko Hattori for their help in the preparation of the recombinant proteins. We thank the beamline staff at the Photon Factory and SPring-8 for providing data-collection facilities and support.

Funding information

Funding for this research was provided by: JSPS KAKENHI (grant No. JP19H03361 to Tadashi Satoh); Joint Research by Exploratory Research Center on Life and Living Systems (ExCELLS) (grant No. 19-315 to Tadashi Satoh).

References

Appenzeller, C., Andersson, H., Kappeler, F. & Hauri, H.-P. (1999). *Nat. Cell Biol.* **1**, 330–334.
Chen, V. B., Arendall, W. B., Headd, J. J., Keedy, D. A., Immormino, R. M., Kapral, G. J., Murray, L. W., Richardson, J. S. & Richardson, D. C. (2010). *Acta Cryst.* D**66**, 12–21.
Chen, Y., Hojo, S., Matsumoto, N. & Yamamoto, K. (2013). *Glycobiology*, **23**, 904–916.
Elshorst, B., Hennig, M., Försterling, H., Diener, A., Maurer, M., Schulte, P., Schwalbe, H., Griesinger, C., Krebs, J., Schmid, H., Vorherr, T. & Carafoli, E. (1999). *Biochemistry*, **38**, 12320–12332.
Emsley, P., Lohkamp, B., Scott, W. G. & Cowtan, K. (2010). *Acta Cryst.* D**66**, 486–501.
Fiedler, K., Parton, R. G., Kellner, R., Etzold, T. & Simons, K. (1994). *EMBO J.* **13**, 1729–1740.
Fukamachi, M., Kasamatsu, A., Endo-Sakamoto, Y., Fushimi, K., Kasama, H., Iyoda, M., Minakawa, Y., Shiiba, M., Tanzawa, H. & Uzawa, K. (2018). *Exp. Cell Res.* **368**, 119–125.
Guy, J. E., Wigren, E., Svärd, M., Härd, T. & Lindqvist, Y. (2008). *J. Mol. Biol.* **381**, 941–955.
Hauri, H.-P., Kappeler, F., Andersson, H. & Appenzeller, C. (2000). *J. Cell Sci.* **113**, 587–596.
Kamiya, Y., Kamiya, D., Yamamoto, K., Nyfeler, B., Hauri, H.-P. & Kato, K. (2008). *J. Biol. Chem.* **283**, 1857–1861.
Kamiya, Y., Satoh, T. & Kato, K. (2012). *Biochim. Biophys. Acta*, **1820**, 1327–1337.
Kamiya, Y., Yamaguchi, Y., Takahashi, N., Arata, Y., Kasai, K., Ihara, Y., Matsuo, I., Ito, Y., Yamamoto, K. & Kato, K. (2005). *J. Biol. Chem.* **280**, 37178–37182.
Kornfeld, R. & Kornfeld, S. (1985). *Annu. Rev. Biochem.* **54**, 631–664.
Krissinel, E. & Henrick, K. (2004). *Acta Cryst.* D**60**, 2256–2268.
Krissinel, E. & Henrick, K. (2007). *J. Mol. Biol.* **372**, 774–797.
McCoy, A. J., Grosse-Kunstleve, R. W., Adams, P. D., Winn, M. D., Storoni, L. C. & Read, R. J. (2007). *J. Appl. Cryst.* **40**, 658–674.
Murshudov, G. N., Skubák, P., Lebedev, A. A., Pannu, N. S., Steiner, R. A., Nicholls, R. A., Winn, M. D., Long, F. & Vagin, A. A. (2011). *Acta Cryst.* D**67**, 355–367.
Naismith, J. H. & Field, R. A. (1996). *J. Biol. Chem.* **271**, 972–976.
Nishio, M., Kamiya, Y., Mizushima, T., Wakatsuki, S., Sasakawa, H., Yamamoto, K., Uchiyama, S., Noda, M., McKay, A. R., Fukui, K., Hauri, H.-P. & Kato, K. (2010). *Proc. Natl Acad. Sci. USA*, **107**, 4034–4039.
Otwinowski, Z. & Minor, W. (1997). *Methods Enzymol.* **276**, 307–326.
Satoh, T., Cowieson, N. P., Hakamata, W., Ideo, H., Fukushima, K., Kurihara, M., Kato, R., Yamashita, K. & Wakatsuki, S. (2007). *J. Biol. Chem.* **282**, 28246–28255.
Satoh, T., Suzuki, K., Yamaguchi, T. & Kato, K. (2014). *PLoS One*, **9**, e87963.
Vagin, A. & Teplyakov, A. (2010). *Acta Cryst.* D**66**, 22–25.
Velloso, L. M., Svensson, K., Schneider, G., Pettersson, R. F. & Lindqvist, Y. (2002). *J. Biol. Chem.* **277**, 15979–15984.
Wigren, E., Bourhis, J.-M., Kursula, I., Guy, J. E. & Lindqvist, Y. (2010). *FEBS Lett.* **584**, 878–882.
Yagi, H., Yagi-Utsumi, M., Honda, R., Ohta, Y., Saito, T., Nishio, M., Ninagawa, S., Suzuki, K., Anzai, T., Kamiya, Y., Aoki, K., Nakanishi, M., Satoh, T. & Kato, K. (2020). *Nat. Commun.* **11**, 1368.
Zhang, B., Cunningham, M. A., Nichols, W. C., Bernat, J. A., Seligsohn, U., Pipe, S. W., McVey, J. H., Schulte-Overberg, U., de Bosch, N. B., Ruiz-Saez, A., White, G. C., Tuddenham, E. G., Kaufman, R. J. & Ginsburg, D. (2003). *Nat. Genet.* **34**, 220–225.
Zhang, B., McGee, B., Yamaoka, J. S., Guglielmone, H., Downes, K. A., Minoldo, S., Jarchum, G., Peyvandi, F., de Bosch, N. B., Ruiz-Saez, A., Chatelain, B., Olpinski, M., Bockenstedt, P., Sperl, W., Kaufman, R. J., Nichols, W. C., Tuddenham, E. G. & Ginsburg, D. (2006). *Blood*, **107**, 1903–1907.
Zhang, B., Spreafico, M., Zheng, C., Yang, A., Platzer, P., Callaghan, M. U., Avci, Z., Ozbek, N., Mahlangu, J., Haw, T., Kaufman, R. J., Marchant, K., Tuddenham, E. G., Seligsohn, U., Peyvandi, F. & Ginsburg, D. (2008). *Blood*, **111**, 5592–5600.
Zheng, C., Page, R. C., Das, V., Nix, J. C., Wigren, E., Misra, S. & Zhang, B. (2013). *J. Biol. Chem.* **288**, 20499–20509.
Zhu, M., Zheng, C., Wei, W., Everett, L., Ginsburg, D. & Zhang, B. (2018). *Blood Adv.* **2**, 1014–1021.